Available online at www.sciencedirect.com

jmr&t Journal of Materials Research and Technology

https://www.journals.elsevier.com/journal-of-materials-research-and-technology

Original Article

Kinetic modeling of the leaching of $LiCoO_2$ with phosphoric acid

Eliana G. Pinna[a,c], *D. Sebastián Drajlin*[a], *Norman Toro*[b,d,e], *Mario H. Rodriguez*[a,*]

[a] *Laboratorio de Metalurgia Extractiva y Síntesis de Materiales (MESiMat), Instituto Interdisciplinario de Ciencias Básicas, Universidad Nacional de Cuyo, CONICET, Facultad de Ciencias Exactas y Naturales, Padre J. Contreras 1300, 5500, Mendoza, Argentina*

[b] *Faculty of Engineering and Architecture, Universidad Arturo Prat, Almirante Juan José Latorre 2901, Antofagasta 1244260, Chile*

[c] *Facultad de Ciencias Agrarias, Universidad Nacional de Cuyo, Alte. Brown 500, 5505, Mendoza, Argentina*

[d] *Departamento de Ingeniería Metalúrgica y Minas, Universidad Católica del Norte, Antofagasta 1270709, Chile*

[e] *Department of Mining and Civil Engineering, Universidad Politécnica de Cartagena, 30203 Cartagena, Spain*

ARTICLE INFO

Article history:
Received 30 May 2020
Accepted 24 September 2020
Available online 8 October 2020

Keywords:
$LiCoO_2$
Kinetic model
LIBs
Surface chemical reaction.

ABSTRACT

In this article, we analyze the leaching kinetics with phosphoric acid of $LiCoO_2$ samples from spent Li-ion batteries and commercial $LiCoO_2$. The purpose was to study the mechanism by which the extraction reaction of cobalt and lithium is produced from the solid samples. The experimental results showed that raising the temperature and the reaction time contributed to improving both the extraction of Li and Co from the structure. The leaching rate of the metals from both samples in the phosphoric acid solution could be expressed as: $\ln(1-X) = -b_1\left[\ln(1+b_2t) - \frac{b_2t}{1+b_2t}\right]$. The morphology of the solid revealed that the dissolution reaction of the samples develops from preferential growth of active sites, points susceptible to chemical interaction, occurring in one direction, giving rise to the start and progress of the reaction. The generation of these sites in the LCO-H_3PO_4 reaction system is of the ẗsequentialẗype. The apparent activation energy values for the leaching of Co and Li would indicate that the surface chemical reaction is the rate-controlling step during this dissolution process.

© 2020 The Author(s). Published by Elsevier B.V. This is an open access article under the CC BY-NC-ND license (http://creativecommons.org/licenses/by-nc-nd/4.0/).

1. Introduction

In hydrometallurgical processes, used for the extraction and recovery of metals, it is essential to study the reaction kinetics, since it allows us to identify the reaction mechanism and to design more efficient equipment and processes. In addition, hydrometallurgical processes operate at lower temperatures than those used, for example, in pyrometallurgical processes, which generally leads to lower reaction rates and the limitations found are mainly kinetic [1,2].

In recent decades, electronic devices have become a fundamental part of daily life. The accelerated technological development, along with their short lifespan, bring about an increase in the replacement of these devices and the accumulation of disused ones. According to Shaikh et al. [3]

* *Corresponding author.*
E-mail: mrodriguez@uncu.edu.ar (M.H. Rodriguez).

https://doi.org/10.1016/j.jmrt.2020.09.109

2238-7854/© 2020 The Author(s). Published by Elsevier B.V. This is an open access article under the CC BY-NC-ND license (http://creativecommons.org/licenses/by-nc-nd/4.0/).

Table 1 – Summary of published works on the leaching kinetics of cathodic materials.

*Ref.	Sample	Leached agent	Reductor agent	Reaction control	Activation energy ($kJmol^{-1}$)
[7]	LCO	HCl	----------	Surface chemical reactions	Li: 23.83 Co: 27.72
[8]	LCO		----------	----------	Stages I and II: Co: 40 and 20 Li: 17 and 9
[9]	LCO LMO NMC	H_3PO_4	H_2O_2	Chemical reaction and internal diffusion	Li: 37.74 Li: 21.16 Li: 21.86
[10]	LCO			----------	Li: 10.16 Co: 7.30
[11]	Cathode and anode scraps LCO	H_2SO_4	H_2O_2	Surface chemical reaction	Mn: 30.1 Ni: 36.7 Co: 41.4 Li: 37.4
[12]	LCO			Co chemical reaction and Li internal diffusion	Li: 32.4 Co: 59.8
[13]	LCO NMC		$NaHSO_3$	Diffusion	Li: 20.4 Co: 26.8 Ni: 21.7
[14]	LCO NMC		----------	Diffusion	Li: 16.4 Co: 7.4 Mn: 18.5
[8]	LCO		----------	----------	Stage I and II: Co: 43 and 3 Li: 16 and 6
[15]	Cathode scraps NMC	Trichloroacetic acid Acetic acid	H_2O_2	Residue layer diffusion and surface chemical reaction	Co: 54.22 Ni: 53.21 Mn: 55.68 Li: 52.04
[16]		Trichloroacetic acid		Chemical reaction control	Mn: 43.8 Li: 28.0 Co: 44.7 Ni: 44.5
[17]	Cathode scraps NMC	Formic acid	---------	Surface chemical reaction	Co: 41.52 Mn: 41.64 Ni: 41.16 Li: 43.61
			H_2O_2		Co: 37.17 Mn: 39.38 Ni: 38.47 Li: 38.29
[18]	LCO			Surface chemical reaction	Li: 44.12 Co: 51.75
[19]	NMC	Malic acid	Electrochemical reduction	----------	Li 41.71 Ni: 42.83 Co: 44.38 Mn: 43.17
[20]	Cathode scraps NMC	NH_3 $(NH_4)_2SO_4$ Na_2SO_3	----------	Surface chemical reaction	Li: 83.3 Ni: 77.9 Co: 87.9
[21]	LCO NMC LMO	Citric acid	H_2O_2	Chemical reaction	Mn: 45.0 Li: 66.0 Co: 86.0 Ni: 49.0
[22]	LCO			Diffusion reaction control	---------
[23]	LCO NMC	L-Tartaric acid	H_2O_2	Chemical reaction control	Mn: 66.0 Li: 54.0 Co: 58.0 Ni: 73.0

– Table 1 (*Continued*)

*Ref.	Sample	Leached agent	Reductor agent	Reaction control	Activation energy ($kJmol^{-1}$)
[24]	LCO	Succinic acid	H_2O_2	Surface chemical reaction and layer diffusion	
[25]	NMC	Lactic acid	H_2O_2	Surface chemical reaction	Li: 62.81 Mn: 70.62 Ni: 63.96 Co: 62.83

approximately 52.7 million tons of electronic waste will be generated worldwide in 2021.

Although electronic waste (e-waste) accounts for only 3 to 5% of solid waste, its variety and content of valuable metals and plastics exceed those of other forms of municipal waste, which is why they are called "Urban Mining". Within the e-waste, portable electronic equipment has batteries (Li-ion, Ni-MH, Ni-Cd) that usually contain a large number of valuable metals (Li, Co, Ni, Mn, Cd, Fe, Al, Cu, etc.) and organic compounds that can be dangerous to the environment [4].

In Li-ion batteries, Li^+ ions migrate from the cathode to the anode during charging and vice versa during discharge. Usually, intercalated compounds of lithium mixed oxides are used, such as $LiCoO_2$ (LCO), $LiNi_xCo_yMn_zO_2$ (NCM, x + y+z = 1), $LiNi_xCo_yAl_zO_2$ (NCA, x + y+z = 1), $LiMn_2O_4$ (LMO) as active cathode materials. Graphite is the solid used in the anodes. In both electrodes, the solids adhere to a metallic sheet (aluminum for the cathode and copper for the anode) with fluoro-polyvinylidene (PVDF) and are embedded in an electrolyte. Furthermore, both electrodes are separated by a plastic film and covered by a metal casing [5,6].

The global battery market is projected to reach $ 100 billion in 2025 [6]. That is why numerous investigations study processes for the recycling of these devices. One of the most studied routes is hydrometallurgy, whose purpose is to extract the metals present in the different parts of the batteries by the action of a leaching agent and then to recover said metals by chemical precipitation, electrodeposition, among others [5]. As mentioned earlier, the kinetic study in these processes has particular importance in the elaboration of kinetic models that describe the mechanisms of leaching of the metals to optimize the process and turn it into an efficient source for obtaining different metals.

Table 1 presents a summary of the main results, reported in the bibliography, on the kinetic aspects of the dissolution reaction of the cathodic material of LIBs in different leaching media.

In Table 1, it is observed that the reaction rate of the reacting systems (cathodic material/leaching agent/reducing agent) can be controlled chemically or physically depending on the type of leaching agent used. In general, moderate or weak acids have chemical control over the reaction rate, regardless of the cathodic material used. In contrast, strong acids such as sulfuric or hydrochloric showed a diffusion-type reaction control; although in the latter case the E_a values depend on the type of metal extracted, having the Co higher E_a values than the Li. In all the investigations reported in the bibliography, activation energies were only determined using the Arrhenius equation, after adjusting the experimental results, extraction versus time at different temperatures, with traditional linear-type equations such as those proposed by Levenspiel in the decade of the 1960s [26].

In the bibliography, two works have been reported whose experimental design has the purpose of studying the operational parameters of the dissolution of LCO with H_3PO_4 [9,10]. Afterward, the authors took advantage of the results to carry out a kinetic study through which they obtained the E_a values for Li [9,10] and Co [10]. According to their investigations, the authors used long initial periods, high temperatures and high concentrations of H_3PO_4 and H_2O_2. This led to obtaining high values of initial conversions (X) that led to a fit of the kinetic model with high regression errors (R^2). So much so, Chen et al. [10] reported an R^2 of 0.85 for Co (E_a 7.3 kJ mol^{-1}) and 0.92 for Li (E_a 10.16 kJ mol^{-1}). These low adjustment values (R^2) would indicate that the chosen model does not explain all the variability of the results obtained, transferring this error to the reported E_a values [9,10]. Also, the type of reaction control and the mechanism by which the reaction takes place are not particularly studied. Furthermore, according to the literature, the most appropriate way to evaluate the kinetic behavior of the chemical reaction is to perform it at low conversions, X, (if possible at X < 0.1). To achieve this in the experimental design, it is necessary (mainly) to obtain information about the effect of time and temperature on the reaction rate at short periods and low temperatures, at concentrations of leaching and reducing agent slightly above the stoichiometric values calculated from the LCO dissolution reaction. This will allow us to obtain results or data at the beginning of the reaction which will be very important and will be reflected in the form of the model fit curve (X vs time at different temperatures) from which the kinetic parameters will be calculated (e.g. k and E_a) [27].

That is why this work proposes to carry out a comparative kinetic study of two LCO samples, one from LIBs and the other commercial, to propose a reaction mechanism for both solids. Furthermore, we aim to determine the E_a for Li and Co for both samples using the M̈ODELADOs̈oftware, which correlates the experimental results of Li and Co extraction, at different times and temperatures, with mathematical models whose formulation has many important aspects of the reacting system that traditional models do not. Among them are the shape and size of the solid reacting particle, the evolution and changes that the surface of the reacting particle experiences with the progress of the reaction. The incorporation of these parameters to these mathematical models will allow obtaining more precise values of apparent activation energies for Li and Co. In this sense, we also expect to correct and/or corroborate the results presented in the bibliography.

2. Materials and methods

2.1. Materials

The reagents used, H_3PO_4 and H_2O_2, were of analytical grade, and all the solutions were prepared with specified concentrations in distilled water. The samples were: $LiCoO_2$ obtained from cathodes of LIBs of mobile phones of different brands and models identified as M1 and commercial $LiCoO_2$ identified as M2.

2.2. Analytical methods and experimental procedure

The reagents and products were characterized by X-ray diffraction (XRD) with a diffractometer Rigaku D-Max III C, scanning electron microscopy (SEM) in a microscope LEO 1450 VP which was equipped with an X-ray dispersive spectrometer EDAX Genesis 2000. The composition quantitative determinations of the sample were performed by atomic absorption spectroscopy (AAS) using a Varian SpectrAA 55 spectrometer and X-ray fluorescence (XRF) on a Shimadzu EDX 7000 instrument. The surface area was also analyzed using the BET method in a Micromeritics Gemini V.

Table 2 – Atomic percentage of the sample composition.

Elements (%)	Li	Co	Mn	Ni	Al	Fe	C
M1	7.4	54.6	2.1	1.8	0.3	0.2	0.9
M2	8.1	55.9	1.9	1.4	-----	-----	-----

The atomic percentage of the sample composition is shown in Table 2, as determined by AAS (Li) and XRF (Co, Al, Fe, Mn, C and Ni).

The leaching tests were performed in a closed batch reactor of 800 mL built in Teflon® and equipped with magnetic stirring and temperature control systems. Fig. 1 presents a flow diagram of the process.

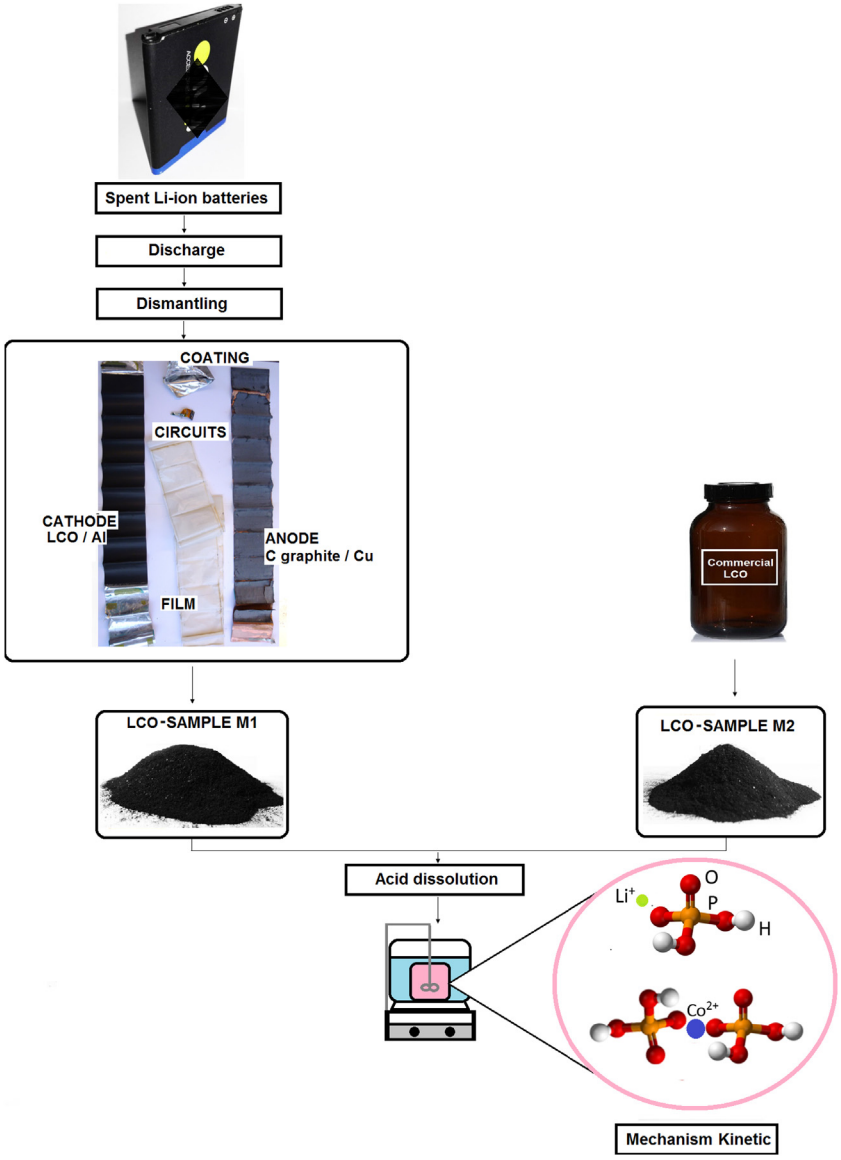

Fig. 1 – Process flow diagram.

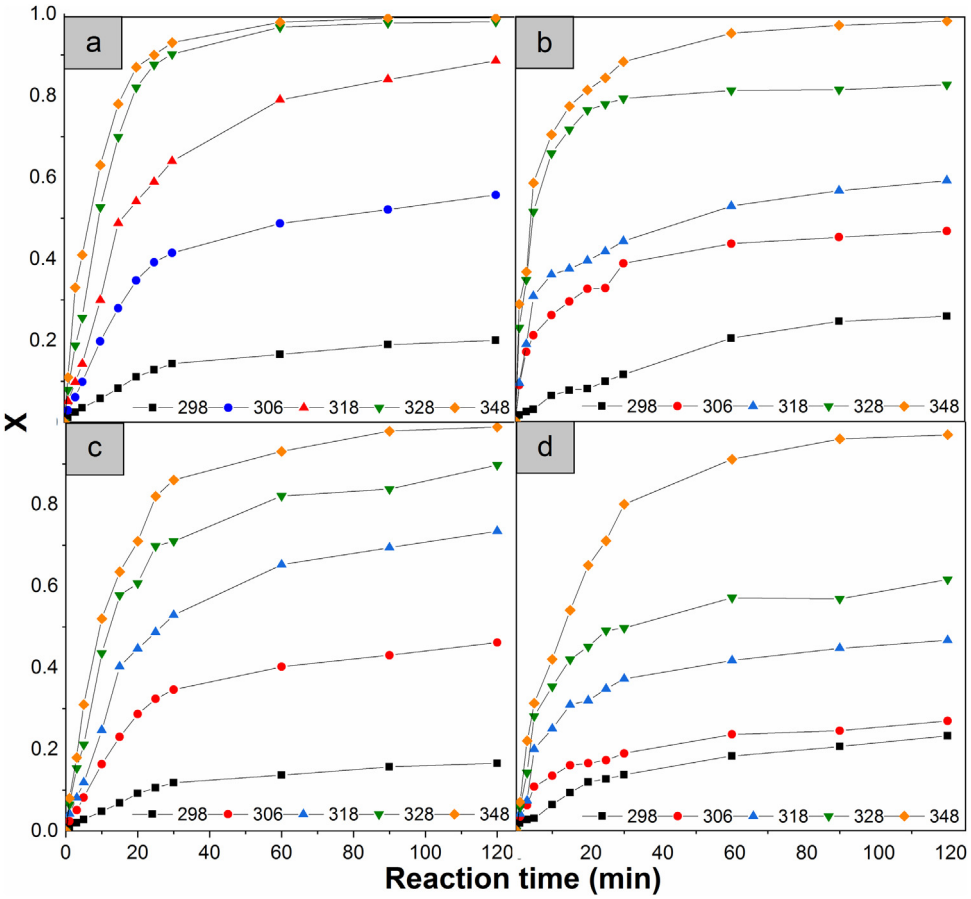

Fig. 2 – Effect of time on the dissolution reaction rate of samples at different temperatures.

For each test, calculated amounts of $LiCoO_2$ (M1 or M2) and distilled water were introduced into the reactor. This mixture was heated to attain the working temperature. Subsequently, a calculated volume of H_3PO_4 was added and the reaction time began to be measured. The leaching tests were carried out under conditions optimized by Pinna et al. [28], H_3PO_4 concentration, 2% v/v; H_2O_2 concentration, 2% v/v; stirring speed, 330 rpm and solid-liquid ratio, 8 g L^{-1}. All the experiments were performed in triplicate to avoid random errors.

3. Results and discussion

3.1. *Effect of temperature and reaction time*

The dissolution tests were conducted under the following conditions: H_3PO_4 concentration, 2% v/v; H_2O_2 concentration, 2% v/v; stirring speed, 330 rpm and solid-liquid ratio, 8 g L^{-1}. The effect of varying the temperature and the reaction time on the dissolution of metals contents in the sample (M1 and M2) was investigated between 298 and 348 K and 0.5–120 min. These results are shown in Fig. 2, where the percentage of leaching of the metals was used to determine the kinetics of the dissolution reaction.

In Fig. 2 can be observed that the dissolution rate (X) has significantly increased until 30 min. After this period, the increase in the response is slight until the curve reaches the plateau at 120 min. Furthermore, the differences in the extraction of Li and Co and in the LCO leaching rate between both samples M1 and M2 could be mainly attributed to the difference in their reactivities. Therefore, the lower reactivity of the M2 sample is justified in its structure being fresh, that is, it has not been used as a means of energy transport. While the structure of sample M1 has been subjected to several charge and discharge cycles in which Li^+ enters and leaves it (intercalation reaction). This migration of Li ions from the cathode to the anode would mainly produce a distortion in the crystal lattice (structure) to compensate for the deficiency of positive charge. The repetition of this process causes wear on the structure of the cathode material (LCO-M1), which creates permanent modifications in the original crystal lattice of the LCO, thus generating vulnerable or preferential sites for the attack of the chemical agent. These sites could be due to Schottky or Frenkel defects, such as crystalline defects, charge deficient sectors due to migration of Li ions to interstitial sites, and distortion or stresses of the LCO crystal lattice. This leads to an increase in the rate and extraction values of Li and Co for the M1 sample [27–30].

In Fig. 2, it can also be seen that in both samples Li has a higher extraction speed than Co. This may be related to the fact that lithium is extracted from the solid in the same way in which it is (Li^+), while Co would need an additional step of reducing Co^{3+} to Co^{2+} to be leached. In the latter case, sample

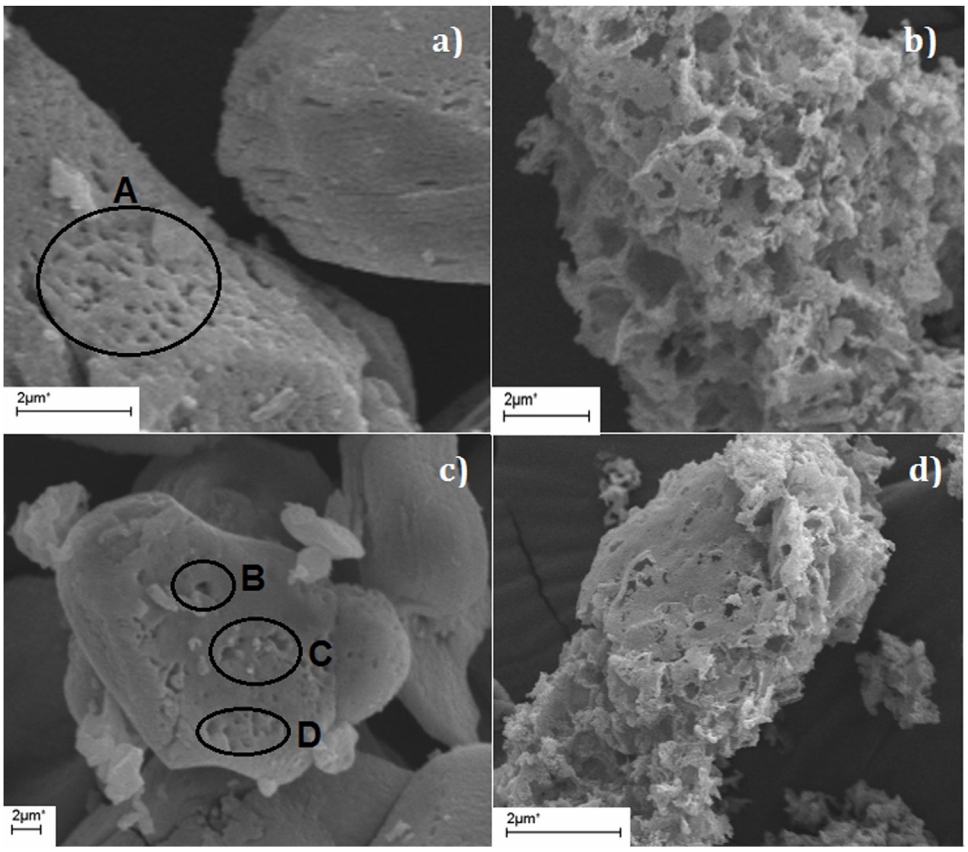

Fig. 3 – SEM micrographs of the residues from the samples M1 (a and b) and M2 (c and d) leached for different periods.

M2 presents additional resistance related to the freshness of its structure.

3.2. *Characterization of leaching residues*

The analysis was performed using SEM to infer what type of chemical attack the samples suffer. For this, the residuals of both samples where the conversion was less than 40% were analyzed. In Fig. 3 a) and c), SEM micrographs of M1 and M2 residues leached for 1 min at 298 K, respectively, are shown. In them, it can be seen that there was a selective attack on certain preferential zones (A, B, C and D) of the particles (holes). In Figs. 3 b) and d), SEM micrographs of M1 and M2 residues leached for 15 min at 298 K, respectively, are shown. In these, a growth in the size of the holes can be observed with respect to Figs. 3 b) and d) at 1 min, which would indicate a progress of the reaction.

Fig. 4 shows the diffractograms of samples M1 (Fig. 4 a) and M2 (Fig. 4 b) before and after leaching. The diffractograms show the peaks corresponding to $LiCoO_2$ (ICDD 01-077-1370) before and after leaching for different periods. The only appreciable difference is the intensity of the peaks according to the degree of dissolution of the sample. The same behavior is observed for sample M2.

The BET method was used to determine the specific surface area of some residues with different degrees of conversion. No important changes were observed on the specific surface area of the residues. The samples M1 and M2 had surfaces ranging from 2 to about 20 $m^2\ g^{-1}$ depending on the progress of the reaction. The increase in surface area would be due to the fact that the LCO dissolution reaction starts at a preferential point of attack (Schottky or Frenkel defects [30]), which then transforms into a hole that grows as the reaction progresses to produce the division of the solid leading to a decrease in the grain size and with it the increase of the surface area. The surface area of 20 $m^2\ g^{-1}$ corresponds to the M1 sample with the longest reaction time.

3.3. *Kinetics analyses*

3.3.1. *Mathematical model*

The kinetic study was performed with the software MODELADO [31] using the experimental data from the study of the effect of temperature and reaction time on the dissolution of the metals contained in the sample (M1 and M2) between 298 and 328 K and between 0.5 and 120 min. (Fig. 2). These data were correlated with 24 different mathematical models. The operational conditions used for each assay were entered as a set of inputs to start the estimation [31]. Then, the software adjusts each of these mathematical models with the experimental data, from which it calculates the regression errors associated with each temperature level. Those models that have a regression error >5% are rejected by the software. Table 3 presents the mathematical models with the lowest percentual regression error values ε(%).

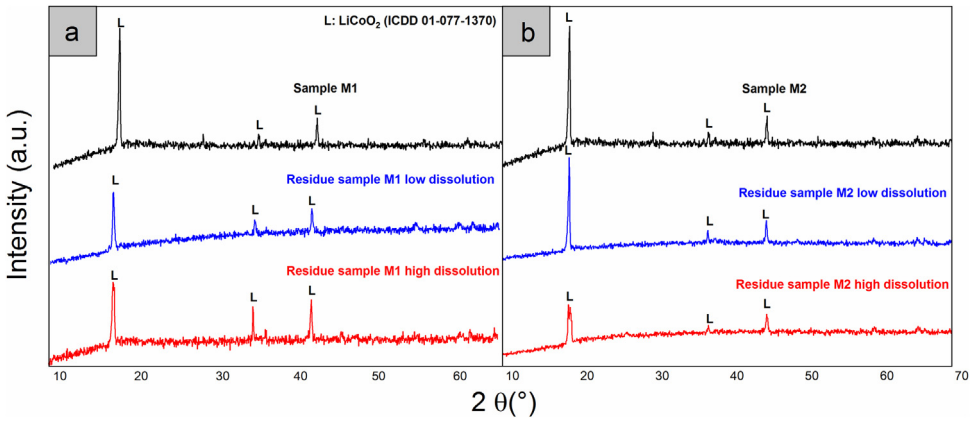

Fig. 4 – Diffractograms of the residues of both samples leached for different periods.

Table 3 – Feasible models according to the percentual regression error.

	Mathematical models			
	Li		Co	
ε (%)	M1	M2	M1	M2
<1	--------	--------	-------	--------
<2	--------	--------	--------	--------
<3	$\ln(1-X) = -b_1\left[\ln(1+b_2t) - \frac{b_2t}{1+b_2t}\right]$ (1)			
<4	--------	--------	--------	$X = b_1\left[\ln(1+b_2t) - \frac{b_2t}{1+b_2t}\right]$ (2)
<5	$X = b_1[1-(1+b_2t)e^{-b_1t}]$ (3) $\ln(1-X) = -b_1[1-(1+b_2t)e^{b_2t}]$ (4)	$\ln(1-X) = -b_1[1-(1+b_2t)e^{b_2t}]$ (4)		$\ln(1-X) = -b_1[1-(1+b_2t)e^{b_2t}]$ (4)

The feasible kinetic models (Table 3) are based on the "nucleation and growth of nuclei" theory, which was originally developed for the modeling of transformation reactions and solid decomposition [32–34]. Delmon [35], adapted this theory to fluid-solid reactions, changing the concept of "nucleation" and the "growth of nuclei" to "activation in active sites" and "growth of holes", respectively.

The models of the Eqs. (3) and (4) have a nucleation parameter equal to 1, this value indicating that the nucleation is constant, unlike the models of the Eqs. (1) and (2) whose nucleation parameter is equal to 2, which indicates that the nucleation is of a sequential type, which can be corroborated in Fig. 3. From the regression error of each of the models and considering that the extraction of lithium and cobalt from the structure, in both samples, fit with the same model, the model given in Eq. (1) was selected as the most probable, since it also satisfies the hypotheses of its formulation [27].

The results of experimental data adjustment of the dissolution of the samples M1 and M2 in H_3PO_4 with the selected model are shown in Fig. 5. It can be noted that the experimental results and the values predicted by the kinetic model are in excellent agreement, as observed in the values of the squared correlation coefficient, R^2.

For the deduction of the selected model, the number and rate of generation of spontaneous active sites were proposed. As regards this model, the generation of these sites in the LCO-H_3PO_4 reaction system is that of the s̈equentialẗype [27].

Each model is classified according to assumptions regarding the reactant particle: its reactivity, starting structure, and the changes experienced during the process of transformation [2,36–38].

The selected model has the following hypotheses about the reactant particle:

a) The particle is composed of a non-porous pure solid;
b) There is no formation of solid products remaining on the particle;
c) The interface surface is identical to the surface of the reactant particle;
d) The initial reaction rate of the process is controlled by the rate of formation of the reaction interface.

As regards the formation of the reaction interface, the following two cases should be distinguished: topochemical reactions and reactions that proceed by activation of the interface area. In addition, each formulated model has several particular hypotheses that make them differ from each other.

Eq. (1) is obtained from the following basic equation of growth nuclei and growth of the nuclei theory:

$$\frac{dX}{dt} = \frac{\Omega^0 V_G r_N}{V^0}(1-X) \quad (5)$$

where: Ω^0 is the initial surface of the particle and V^0 its initial volume; r_N is the activation rate of active sites per unit area;

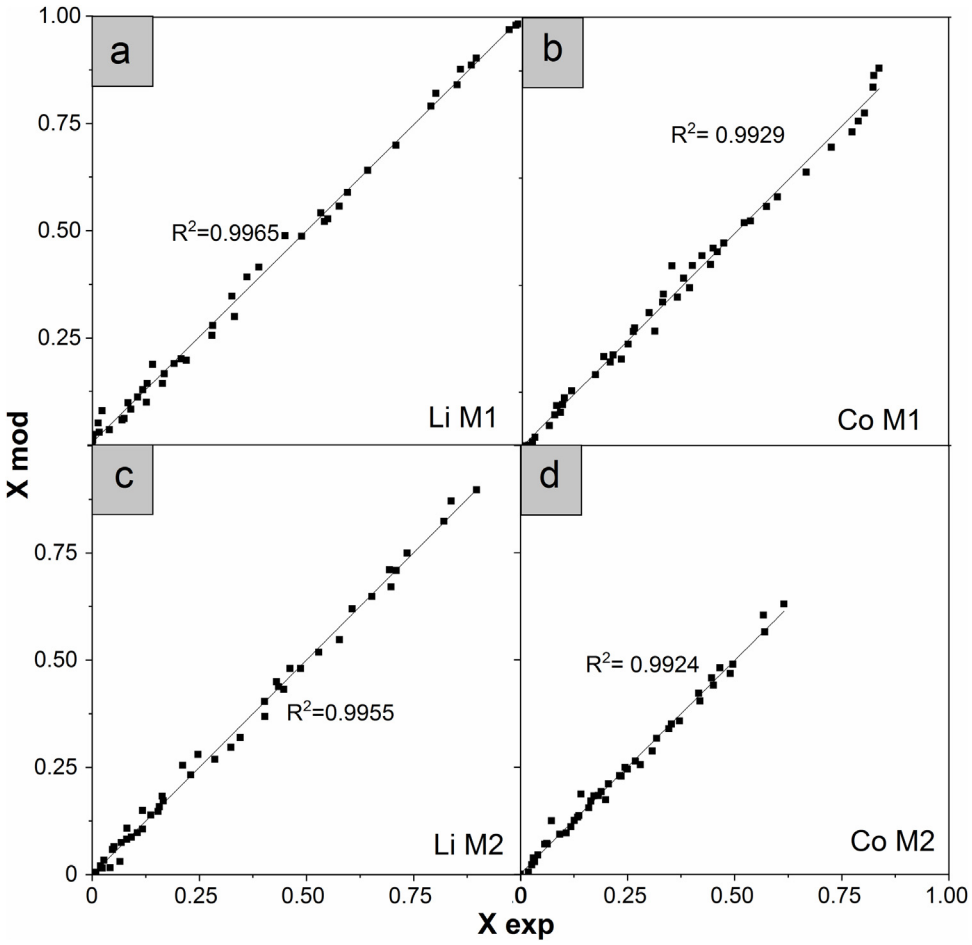

Fig. 5 – Mathematical fit of the dissolution experimental data and kinetic model data.

V_G is the volume of the hole, which, for a time t, is calculated as:

$$V_G = \sigma_g V^0 \left(\frac{bM_B r_S t}{\rho d_p^0} \right)^p \quad (6)$$

where: p, is the growth factor, whose value indicates the direction in which the growth of the nuclei progresses. In the specific case of the model represented by Eq. (1), the value of p is equal to 1, which indicates that the growth of the nuclei is in only one direction, which is consistent with that observed in the micrographs of Fig. 3.

The activation rate, r_N, is defined as:

$$r_N = \frac{k_N N_S^{0\,2} N_E^{0\,m}}{\left(1 + k_N N_S^{0\,2} N_E^{0\,m} t\right)^2} \quad (7)$$

where: N_E^0 it is the number of moles per unit area of a chemical species E that participates in the process, whose identity arises from analyzing different kinetic mechanisms that can be postulated concerning the formation of the reaction interface.

The Eq. (1) corresponds to the particular case of sequential activation of spontaneous active sites, N_S, due to an adsorption-reaction-desorption process, whose rate of change is given by Eq. (8). This is evidenced by the fact that the points of attack do not occur uniformly throughout the surface of the particle, which would occur if it were an instant nucleation, but in localized sectors of it.

$$\frac{dN_s}{dt} = k_N N_E^{0\,m} \left(N_S^0 - N_S \right)^2 \quad (8)$$

where: N_S is the number of activated sites per unit area and m is the order of reaction with respect to species E.

To identify the chemical species E, Eq. (8), it is presumed that the overall rate of the sample dissolution process is controlled by the adsorption stages of the fluid reagent and the chemical reaction, according to the proposed kinetic mechanism, Fig. 6, which takes place on the surface of the sample solid reagent, assuming that m = 2. The proposed mechanism consists of three stages. The first stage is a very rapid reaction where hydrogen peroxide reduces Co^{3+} to Co^{2+} in the presence of diacid phosphate anion, producing the destabilization of the crystal lattice. Then, at a slow stage, chemical adsorption of two $H_2PO_4^-$ molecules occurs on the exposed surface of the solid, more precisely on the lithium and cobalt atoms to form lithium diacid phosphate, which diffuses into the solution and the intermediate $[(Co^{2+})(H_2PO_4^-)]^+$. Finally, in a fast stage, another molecule of $H_2PO_4^-$ reacts with the intermediate forming the cobalt (II) diacid phosphate, which also

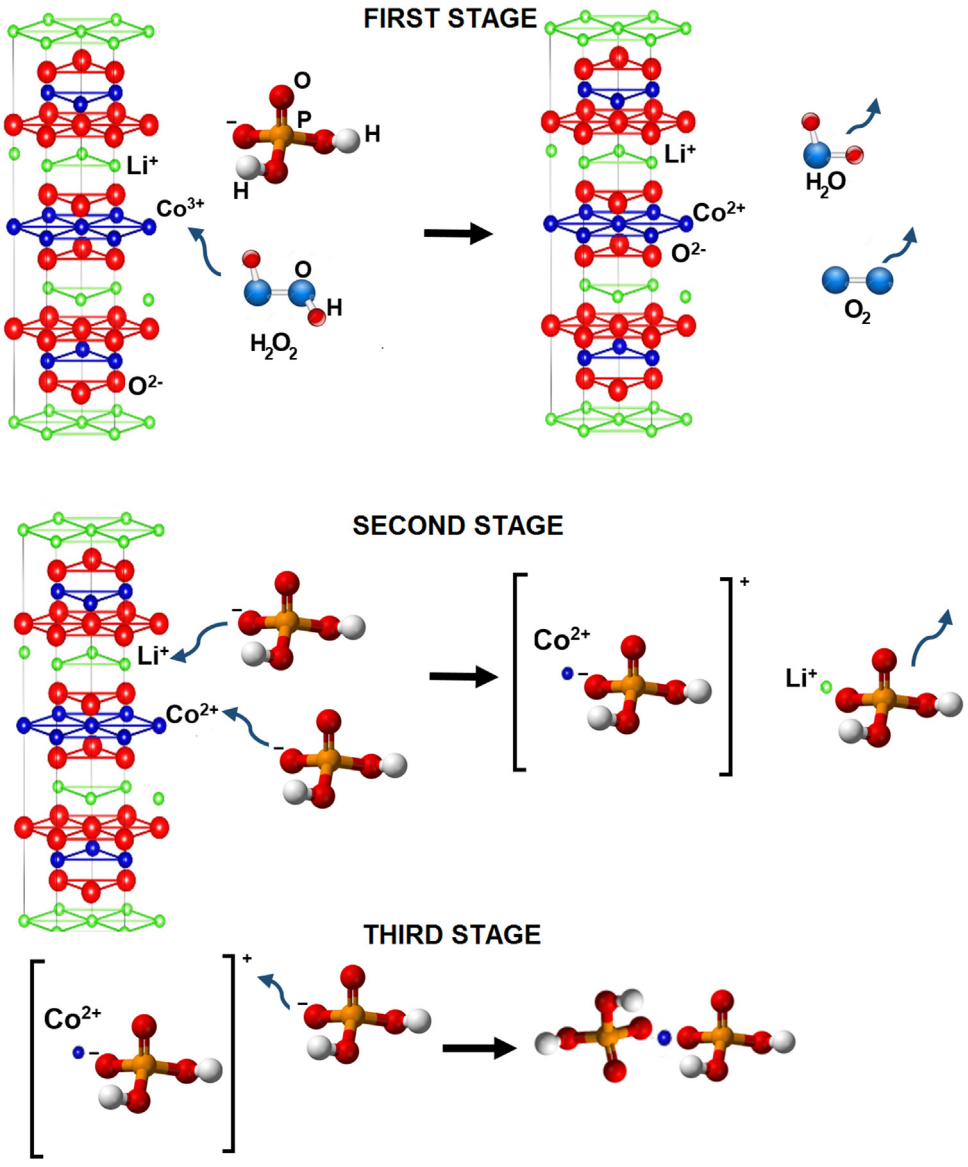

Fig. 6 – Mechanism proposed for the dissolution of LCO with H_3PO_4.

diffuses into the solution. Both phosphates, when diffusing into the solution, leave reaction nuclei from which the attack of the leaching agent would continue. According to the proposed mechanism, Fig. 6, Eq. (7) corresponds to the particular case of a second-order activation speed, where the chemical species E is identified and corresponds to $H_2PO_4^-$. Then, Eq. (6) is expressed as:

$$\frac{dN_S}{dt} = k_N c_{A_S}^2 \left(N_S^0 - N_S\right)^2 \tag{8}$$

where: N_S^0, represents the number of initial moles of the sample per unit of initial surface area of the particle; N_S, is the number of moles of the sample that have been removed since the solid and fluid reagents were contacted; C_{A_S} is the concentration of phosphoric acid evaluated on the reaction interface.

If we integrate the Eq. (8) subject to $N_S = 0$, at $t = 0$, the following is obtained:

$$N_S = \frac{k_N c_{A_S}^2 N_S^{0^2} t}{1 + k_N c_{A_S}^2 N_S^0 t} \tag{9}$$

$$\frac{dN_S}{dt} = \frac{k_N c_{A_S}^2 N_S^{0^2}}{\left(1 + k_N c_{A_S}^2 N_S^0 t\right)^2} = r_N \tag{10}$$

Combining the Eqs. (5) and (6), for $p = 1$, and Eq. (9), and by integrating the resulting equation, we obtain Eq. (1), with the coefficients b_1 and b_2, defined by Eqs. (11) and (12), respectively. The coefficients r_S, k (velocity constant) and k_N (velocity constant of nucleation), are defined in Eqs. (13),(14) and (15).

$$\ln(1 - X) = -b_1 \left[\ln(1 + b_2 t) - \frac{b_2 t}{1 + b_2 t}\right] \tag{1}$$

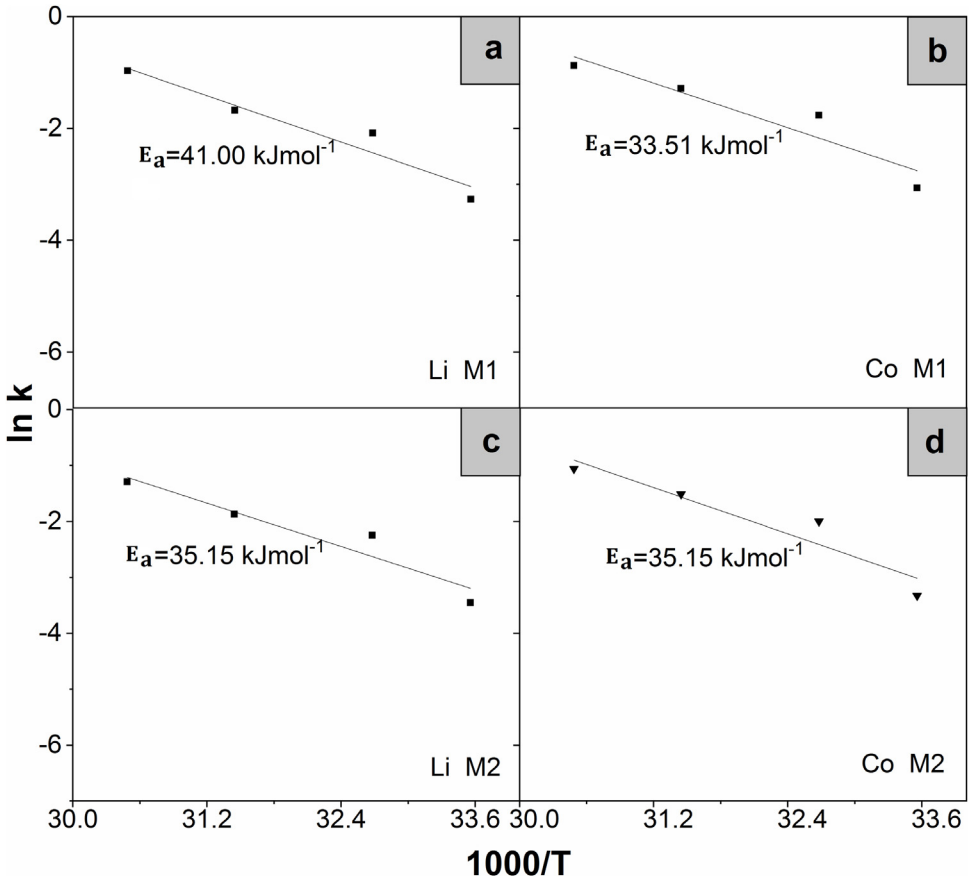

Fig. 7 – Arrhenius plot for the dissolution Li and Co from M1 and M2 LCO in H_3PO_4.

$$b_1 = \frac{\sigma_g N_S^0 \Omega^0 b M_B r_s}{b_2 \rho d_p^0} \quad (11)$$

$$b_2 = k_N N_S^0 \quad (12)$$

$$r_s = k C_{A_s}^n \quad (13)$$

$$k = A_1 e^{\frac{-E_1}{RT}} \quad (14)$$

$$k_N = A_2 e^{\frac{-E_2}{RT}} \quad (15)$$

The reaction control-stage that determines the leaching rate is represented by the value of the activation energy (E_a). When the process is controlled by diffusion stages, the activation energies are less than 12.5 kJ mol^{-1}, since the reaction is slightly temperature-dependent [30]. While processes with activation energies greater than 42 kJ mol^{-1} are chemically controlled and have a strong dependence on the temperature. The E_a was calculated from the slope of the plot of ln k versus 1000/T and results are presented in Fig. 7. The estimated E_a values suggest that the dissolution rate of the oxide for both samples is surface chemical reaction control.

From the results of Figs. 3 and 7, it can be inferred that both samples M1 and M2 experience a topochemical attack and the process is initially controlled by the rate of formation of the reaction interface, through the nuclei that develop in it.

4. Conclusions

The dissolution rate of M1 and M2 increases with increasing temperature and reaction time. The model that best fitted the experimental results is based on the theory of ñuclei and growth of nuclei:. The latter was confirmed by SEM analysis carried out on the attacked particles. In these micrographs it is observed, on the one hand, that the surfaces of the particles that make up samples M1 and M2 are not uniformly reactive and, on the other hand, that the fluid reagent undergoes selective attack at preferential points of said LCO particles. Furthermore, it was inferred that the differences in the extraction values of Li and Co, between M1 and M2, could be attributed to the modifications, distortions and/or deterioration of the original structure of LCO in M1. This occurs due to the continuous wear to which the battery is subjected, during charge and discharge cycles, during its useful life.

The E_a values deduced by the Arrhenius relation were Li, 41.0 and 35.15 kJ mol^{-1} for M1 and M2, respectively, and Co, 33.5 and 35.15 kJ mol^{-1} for M1 and M2, respectively. These E_a values show a chemical type reaction control. Finally, the proposed mechanism for the reaction of dissolution of the LCO (M1 and M2) with phosphoric acid could follow a second order kinetic reaction.

Conflicts of interest

The authors declare no conflicts of interest.

Acknowledgment

The financial support from Universidad Nacional de Cuyo, Secretaria de Investigación, Internacionales y Posgrado (SIIP) and Consejo Nacional de Investigaciones Científicas y Técnicas (CONICET) is gratefully acknowledged.

APPENDIX.

b: Stoichiometric coefficient.

C_a: Concentration of acid evaluated on the interface of reaction, mol L^{-1}.

d^o: Initial particle diameter, μm.

E_a: Activation energy, kJ mol^{-1}.

k: Kinetic coefficient of the reaction rate, m s^{-1}.

k_{N2}: Kinetic coefficient of the formation of the sites, m^2 s^{-1}.

m: Order of reaction with respect to species E.

$N_E{}^0$: Number of moles per unit area of a chemical species E.

$N_S{}^0$: Initial number of the sites that can be activated per unit area of the initial surface of the reactant particle.

N_S: Number of active sites per unit area.

λ: Growth factor.

r_N: Activation sites rate, mol m^{-2} s^{-1}.

r_S: Solid-fluid reaction rate, mol m^{-2} s^{-1}.

T: Temperature, K.

t: Time, s.

t_L: Latency time, s.

τ: Dimensionless time.

v_g: Volume of the hole, m^3.

V_G: Total volume of holes, m^3.

V^0: Initial particle volume, m^3.

X: Degree of dissolution of the solid reactant.

ρ: Solid density, kg m^{-3}.

Ω^0: Initial particle surface, m^2.

σ_g: Shape coefficient of holes.

β: Nucleation order.

ε: Error associated with each level of temperature.

n_r: Stirring speed, rpm.

REFERENCES

[1] Wills BA, Finch J. Wills' mineral processing technology. 8th edition Butterworth-Heinemann; 2016, http://dx.doi.org/10.1016/C2010-0-65478-2.

[2] dos Santos LL, do Nascimento RM, Castellã Pergher SB. Beta-spodumene: Na_2CO_3: NaCl system calcination: a kinetic study of the conversion to lithium salt. Chem Eng Res Des 2019;147:338–45, http://dx.doi.org/10.1016/j.cherd.2019.05.019.

[3] Shaikh S, Thomas K, Zuhair S. An exploratory study of e-waste creation and disposal: upstream considerations. Resour Conserv Recycl 2020;155:104662, http://dx.doi.org/10.1016/j.resconrec.2019.104662.

[4] Zheng X, Zhu Z, Lin X, Zhang Y, He Y, Cao H. Mini-review on metal recycling from spent lithium ion batteries. Engineering 2018;4(3):361–70, http://dx.doi.org/10.1016/j.eng.2018.05.018.

[5] Lv W, Wang Z, Cao H, Sun Y, Zhang Y, Sun Z. A critical review and analysis on the recycling of spent lithium-ion batteries. ACS Sustainable Chem. Eng 2017;6:1504–21, http://dx.doi.org/10.1021/acssuschemeng.7b03811.

[6] Zhang X, Li L, Fan E, Xue Q, Bian Y, Wu F. Toward sustainable and systematic recycling of spent rechargeable batteries. Chem Soc Rev 2018;47:7239–302, http://dx.doi.org/10.1039/c8cs00297e.

[7] Shuva MAH, Kurny ASW. Dissolution kinetics of cathode of spent lithium ion battery in hydrochloric acid solutions. J. Inst. Eng. India Ser. D 2013;94:13–6, http://dx.doi.org/10.1007/s40033-013-0018-0.

[8] Takacova Z, Havlik T, Kukurugya F, Orac D. Cobalt and lithium recovery from active mass of spent Li-ion batteries: theoretical and experimental approach. Hydrometallurgy 2016;163:9–17, http://dx.doi.org/10.1016/j.hydromet.2016.03.007.

[9] Chen X, Cao L, Kang D, Li J, Zhou T, Ma H. Recovery of valuable metals from mixed types of spent lithium ion batteries. Part II: selective extraction of lithium. Waste Manag 2018;80:198–210, http://dx.doi.org/10.1016/j.wasman.2018.09.013.

[10] Chen X, Ma H, Luo C, Zhou T. Recovery of valuable metals from waste cathode materials of spent lithium-ion batteries using mild phosphoric acid. J Hazard Mater 2017;326:77–86, http://dx.doi.org/10.1016/j.jhazmat.2016.12.021.

[11] Nayl AA, Elkhashab RA, Badawy SM, El-Khateeb MA. Acid leaching of mixed spent Li-ion batteries. Arab J Chem 2017;10(2):S3632–9, http://dx.doi.org/10.1016/j.arabjc.2014.04.001.

[12] Jha MK, Kumari A, Jha AK, Kumar V, Hait J, Pandey BD. Recovery of lithium and cobalt from waste lithium ion batteries of mobile phone. Waste Manag 2013;33:1890–7, http://dx.doi.org/10.1016/j.wasman.2013.05.008.

[13] Meshram P, Pandey BD, Mankhand TR. Recovery of valuable metals from cathodic active material of spent lithium ion batteries: leaching and kinetic aspects. Waste Manag 2015;45:306–13, http://dx.doi.org/10.1016/j.wasman.2015.05.027.

[14] Meshram P, Pandey BD, Mankhand TR. Hydrometallurgical processing of spent lithium ion batteries (LIBs) in the presence of a reducing agent with emphasis on kinetics of leaching. Chem Eng J 2015;281:418–27, http://dx.doi.org/10.1016/j.cej.2015.06.071.

[15] Gao W, Song J, Cao H, Lin X, Zhang X, Zheng X. Selective recovery of valuable metals from spent lithium-ion batteries: process development and kinetics evaluation. J Clean Prod 2018;178:833–45, http://dx.doi.org/10.1016/j.jclepro.2018.01.040.

[16] Zhang X, Cao H, Xie Y, Ning P, An H, You H. Scraps of lithium-ion batteries: process optimization and kinetics analysis. Sep Purif Technol 2015;150:186–95, http://dx.doi.org/10.1016/j.seppur.2015.07.003.

[17] Gao W, Zhang X, Zheng X, Lin X, Cao H, Zhang Y. Lithium carbonate recovery from cathode scrap of spent lithium-ion battery: a closed-loop process. Environ Sci Technol 2017;51:1662–9, http://dx.doi.org/10.1021/acs.est.6b03320.

[18] Zheng Y, Song W, Mo W, Zhou L, Liu J. Lithium fluoride recovery from cathode material of spent lithium-ion battery. RSC Adv 2018;8:890–9, http://dx.doi.org/10.1039/c8ra00061a.

[19] Meng Q, Zhang Y, Dong P, Liang F. A novel process for leaching of metals from $LiNi_{1/3}Co_{1/3}Mn_{1/3}O_2$ material of spent lithium ion batteries: process optimization and kinetics aspects. J. Ind. Eng. Chem 2018;61:133–41, http://dx.doi.org/10.1016/j.jiec.2017.12.010.

[20] Zheng X, Gao W, Zhang W, He M, Lin X, Cao H. Spent lithium-ion battery recycling: reductive ammonia leaching of metals from cathode scrap by sodium sulphite. Waste Manag 2017;60:680–8, http://dx.doi.org/10.1016/j.wasman.2016.12.007.
[21] Li L, Bian Y, Zhang X, Guan Y, Fan E, Wu F. Process for recycling mixed-cathode materials from spent lithium-ion batteries and kinetics of leaching. Waste Manag 2018;71:362–71, http://dx.doi.org/10.1016/j.wasman.2017.10.028.
[22] Golmohammadzadeh R, Rashchi F, Vahidi E. Recovery of lithium and cobalt from spent lithium-ion batteries using organic acids: process optimization and kinetic aspects. Waste Manag 2017;64:244–54, http://dx.doi.org/10.1016/j.wasman.2017.03.037.
[23] He L, Sun S, Song X, Yu Y. Leaching process for recovering valuable metals from the $LiNi_{1/3}Co_{1/3}Mn_{1/3}O_2$ cathode of lithium-ion batteries. Waste Manag 2017;64:171–81, http://dx.doi.org/10.1016/j.wasman.2017.02.011.
[24] Li L, Qu W, Zhang X, Lu J, Chen R, Wu F. Succinic acid-based leaching system: a sustainable process for recovery of valuable metals from spent Li-ion batteries. J Power Sources 2015;282:544–51, http://dx.doi.org/10.1016/j.jpowsour.2015.02.073.
[25] Li L, Fan E, Guan Y, Zhang X, Xue Q, Wei L. Sustainable recovery of cathode materials from spent lithium-ion batteries using lactic acid leaching system. ACS Sustainable Chem. Eng 2017;5:5224–33, http://dx.doi.org/10.1021/acssuschemeng.7b00571.
[26] Levenspiel O. Chemical reaction engineering; an introduction to the design of chemical reactors. firth ed New York: John Wiley & Sons; 1962.
[27] Quiroga OD, Avanza JR, Fusco AJ. Modelado cinético de las transformaciones fluido-sólido reactivo. firth ed. Corrientes: Ed. EUDENE; 1996.
[28] Pinna EG, Ruiz MC, Ojeda MW, Rodriguez MH. Cathodes of spent Li-ion batteries: dissolution with phosphoric acid and recovery of lithium and cobalt from leach liquors. Hydrometallurgy 2017;167:66–71, http://dx.doi.org/10.1016/j.hydromet.2016.10.024.
[29] Julien CM, Mauger A, Zaghib K, Groult H. Comparative issues of cathode materials for Li-ion batteries. Inorganics 2014;2:132–54, http://dx.doi.org/10.3390/inorganics2020132.
[30] Habashi F. Principles of extractive metallurgy. Volume I: general principles. second ed. New York: Ed. Gordon and Breach; 1980.
[31] Quiroga OD. Modelado. Software para el tratamiento cinético de transformaciones fluido sólido-reactivo; INIQUI (UNSa-CONICET): salta, Argentina; 2002.
[32] Avrami M. Kinetics of phase change. I general theory. J Chem Phys 1939;7:1103–12, http://dx.doi.org/10.1063/1.1750380.
[33] Avrami M. Kinetics of phase change. II. Transformation-time relations for random distribution of nuclei. J Chem Phys 1940;8:212–24, http://dx.doi.org/10.1063/1.1750631.
[34] Avrami M. Kinetics of phase change. III. Granulation, phase change, and microstructure. J Chem Phys 1941;9:177–84, http://dx.doi.org/10.1063/1.1750872.
[35] Delmon B. Introduction a la cinétique hétérogené. firth ed Paris: Ed. Technip; 1969.
[36] Pinna EG, Barbosa LI, Suarez DS, Rodriguez MH. Kinetic study of the dissolution of metakaolin with hydrofluoric acid. Indian J. Chem. Technol 2018;25:287–93 http://op.niscair.res.in/index.php/IJCT/article/view/12693.
[37] Rosales GD, Ruiz M, Rodriguez M. Study of the extraction kinetics of lithium by leaching β-spodumene with hydrofluoric acid. Minerals 2016;6(4):98, http://dx.doi.org/10.3390/min6040098.
[38] Rodriguez M, Quiroga O, Ruiz MC. Kinetic study of ferrocolumbite dissolution in hydrofluoric acid medium. Hydrometallurgy 2007;85:87–94, http://dx.doi.org/10.1016/j.hydromet.2006.07.005.